The atmospheric impact of the reaction of N2O with NO3: A theoretical study

Thanh Lam Nguyen, Manolis Romanias, A.R. Ravishankara, Aristotelis Zaras, Philippe Dagaut, John Stanton

The Atmospheric Impact of the Reaction of N_2O with NO_3: a Theoretical Study

Thanh Lam Nguyen,[1] Manolis N. Romanias,[2] A. R. Ravishankara,[3,*] Aristotelis M. Zaras,[4] Philippe Dagaut,[4] and John F. Stanton[1,*]

[1]*Quantum Theory Project, Department of Chemistry and Physics, University of Florida, Gainesville, FL 32611 (USA).*

[2]*IMT Lille Douai, Univ. Lille, SAGE – Département Sciences de l'Atmosphère et Génie de l'Environnement, F-59000, Lille, France.*

[3]*Departments of Chemistry and Atmospheric Sciences, Colorado State University, Ft. Collins, CO 80523 (USA). Also associated with the Le Studium, Advanced Institute for Research, Loire Valley, Orleans, France.*

[4]*CNRS-INSIS, Institut de Combustion, Aérothermique, Réactivité et Environnement, 1C avenue de la recherche scientifique, 45071 Orléans cedex 2, France and Université d'Orléans, 6 avenue du Parc Floral, 45100 Orléans, France.*

*Corresponding authors: johnstanton@ufl.edu; A.R.Ravishankara@colostate.edu

The reaction of N_2O with NO_3 is studied for the first time using high-level quantum chemical calculations, followed by statistical rate coefficient estimations. Addition/elimination reaction pathways that lead to the formation of $NO_2 + N_2 + O_2$ and $NO_2 + 2NO$, respectively, have been explored. The formation of $NO_2 + N_2 + O_2$ is found to be exothermic by 30 kcal mol^{-1} while that of $NO_2 + 2NO$ is endothermic by 13 kcal mol^{-1}. Both mechanisms are found to have significant reaction barriers (> 43 kcal mol^{-1}), and the estimated thermal reaction rate constants are very low: about 6×10^{-43} cm^3 $molecule^{-1}$ s^{-1}. Therefore, this reaction is not expected to affect the lifetime of N_2O in the atmosphere.

Introduction

Nitrous oxide, N_2O, is a major greenhouse gas and its emissions are the largest of an ozone layer depleting gas [1]. The main reason for these two distinctions is the long atmospheric lifetime of N_2O (roughly 120 years), which appears not to have any appreciable loss pathway in the troposphere where it is emitted. If there were any reactions in the troposphere that lead to destruction of N_2O – even if very slow – the atmospheric lifetime of this species would be profoundly affected. Therefore, a search for potential slow reactions of tropospheric free radicals with N_2O is of interest.

It is not always easy to directly measure the rate coeffcients for very slow radical-molecule reactions due to various experimental difficulties. These include the need to avoid impurity reactions, unwanted side reactions as well as the use of very large concentrations of N_2O with potential deleterious effects on the ability to detect the radicals. Therefore, assessing the feasibility of slow reactions via theoretical calculations represents an attractive alternative, especially for small molecules. Quantum chemistry calculations have advanced to a stage that it is now fairly straightforward to obtain energetics that are accurate to a few tenths of kcal mol^{-1}. In addition, approaches for calculating rate coefficients using the mapped out potential energy surfaces have advanced, as well. Therefore, we have undertaken a study of the potentially important atmospheric reaction of NO_3 with N_2O. The abundance of NO_3, though highly variable, is sufficiently large that this reaction could have an impact on the lifetime of N_2O if the rate coefficient were of the order of 10^{-20} cm^3 $molecule^{-1}$ s^{-1}, or higher.

Previously, Cantrell et al. [2] attempted to measure this rate coefficient and obtained an upper limit of 2×10^{-17} cm^3 $molecule^{-1}$ s^{-1}. As can be inferred from the preceding, this is not

a sufficiently stringent upper limit to dismiss the possibility that this reaction contributes meaningfully to the loss of N_2O in the atmosphere. Therefore, better estimates are needed. A computational estimation of the rate coefficient for the reaction of NO_3 with N_2O is the goal of this focused study.

Quantum Chemical Calculations

The title reaction involves seven heavy atoms, so high-accuracy HEAT [3-5] calculations would be extremely time consuming; consequently, a compromise is made here. This work is based in part on calculations done with the composite G3B3 method [6], which is a variation of G3 theory [7]. G3B3 [6] uses geometries and harmonic zero-point vibrational corrections obtained at the B3LYP/6-31G(d) level of theory, followed by a series of single-point energy calculations done with methods including QCISD(T)/6-31G(d), MP4/6-31+G(d), MP4/6-31G(2df,p), and MP2/G3Large in order to estimate the QCISD(T) level at the complete basis set limit. In addition, empirical high-level corrections (HLC) and spin-orbit corrections [6] are also included [7]. It is expected that the G3B3 calculations provide (roughly) chemical accuracy (i.e. within 1-2 kcal mol^{-1}) for relative energies. As can be seen in Figure 1, such a level of accuracy is indeed achieved for the reaction enthalpies of two main pathways, and it is expected that this accuracy will not be seriously degraded for transition state (TS) structures. Moreover, intrinsic reaction coordinate (IRC) [8-10] calculations were also performed in order to verify that the located transition state structures properly connect reactant(s) and products. It should be mentioned that NO_3 is a notoriously difficult molecule for both experiment and theory. DFT calculations with B3LYP give a C_{2v} equilibrium geometry for NO_3, although the experimentally determined

ground state average geometry is D_{3h}. Although a comparison of equilibrium geometries with experimental structures is fraught with difficulties, especially for a system of this type, it is true that the potential surface for NO_3 near the minimum is extremely flat. Hence, many methods give symmetric structures while many others give broken symmetry structures. However, the energetics are largely insensitive, owing to the flat nature of the potential. The G3B3 and IRC calculations were done using the Gaussian 09 program suite [11].

In addition to the G3B3 calculations, we have also used high-level coupled-cluster calculations to characterize key stationary points (see Figure 1) for the purpose of chemical kinetics analysis. First, geometries were optimized using the coupled-cluster method with single, double, and perturbative triple excitations (CCSD(T)) [12-14] in combination with the atomic natural orbital double-zeta (ANO0) basis set [15, 16], followed by harmonic vibrational analyses in order to check if they are real minima or first-order saddle points. Second, the ANO0 geometries and Hessian matrix obtained above were used for reoptimizing with a larger triple-zeta (ANO1) basis set [15, 16]. Third, single-point energies were refined using the same CCSD(T) method, but with Dunning's quadruple-zeta basis set [17], cc-pVQZ. Finally, additional minor corrections have been applied for the effects of scalar relativity, the diagonal Born-Oppenheimer correction (DBOC), and spin-orbit coupling. As can be seen in Figure 1, both the simple G3B3 and more elaborate CCSD(T)/cc-pVQZ calculations agree well (within 1-2 kcal mol^{-1}) with one another, although the CCSD(T) values are systematically about 1-2 kcal mol^{-1} lower. A similar difference has been found in the reaction of OH with N_2O [18]. All CCSD(T) calculations are done using the CFOUR quantum chemistry package [19].

Reaction Mechanisms and Energetics

Two pathways have been characterized for the thermal reaction of NO_3 radical with N_2O. The first:

$NO_3 + N_2O \rightarrow NO_2 + N_2 + O_2$; Δ_fH (0 K) = –30.7 kcal mol^{-1} (ref. [20]) (1)

(hereafter defined as pathway 1) is very exothermic [20], and leads to the formation of three stable molecules, NO_2, N_2 and O_2. The second pathway (hereafter defined as pathway 2)

$NO_3 + N_2O \rightarrow NO_2 + 2NO$; Δ_fH (0 K) = +12.6 kcal mol^{-1} (ref. [20]) (2)

is endothermic [20], resulting in NO_2 + 2NO, and therefore is highly unlikely to occur under atmospheric conditions. The G3B3 calculations give –29.9 and 12.9 kcal mol^{-1} for reactions 1 and 2, respectively, which agree within 1 kcal mol^{-1} with both the CCSD(T) calculations and well established thermochemical values [20]. The optimized geometries of various species are given in the supplementary material, while those of key transition states and intermediates along the reaction coordinate obtained with the DFT-B3LYP method are shown in Figure 1. The calculated relative energies including zero-point energy corrections for various species are given in Table 1.

For pathway 1 as presented in Figure 1, NO_3 attacks the oxygen end of N_2O. Initially, a weakly bound pre-reactive complex is formed (Pre-1) with a binding energy of –2.3 kcal mol^{-1} as calcuated with G3B3. This complex then proceeds to abstract an O atom through TS-1 leading to Post-1. The barrier height of TS-1 is calculated to be 51.6 and 49.9 kcal mol^{-1} using the G3B3 and CCSD(T) methods, respectively. Post-1, a post-reaction complex with a relative energy of –31.6 kcal mol^{-1}, when produced, should rapidly

dissociate to the final products, $NO_2 + N_2 + O_2$ driven by the very large entropy increase, together with a negligible barrier and low endothermicity (~ 1 kcal mol^{-1}). According to Figure 1, TS-1 is the key saddle point, because passing over (or through) TS-1 is the rate-determining step. Yet, TS-1 has a large spin contamination ($<S^2>$) of 1.5. So, in addition to UHF-CCSD(T) method, ROHF-CCSD(T) was also used for optimization. A comparison of two optimized geometries are displayed in Figure 2 with the ROHF-CCSD(T) values shown in parentheses. Inspection of Figure 2 shows that the two geometries are in good agreement: there are small differences of 0.015 Å for the O–O bond length and of 0.4 degrees for the ∠NOO angle. However, there is a difference of 2 kcal mol^{-1} (not shown in Figure 1) for the calculated barrier heights, where the ROHF-CCSD(T) method gives a lower value. Because of this, we take the 49.9 kcal mol^{-1} barrier height from ROHF-CCSD(T)/cc-pVQZ, but recognize that it is associated with a relatively large uncertainty (up to perhaps 3-5 kcal mol^{-1}).

For pathway 2 as displayed in Figure 1, NO_3 can attack the nitrogen end of N_2O via TS-2 leading to the formation of an intermediate adduct, INT1. The energy barrier of TS-2 is calculated to be 35.1 and 34.4 kcal mol^{-1} using the G3B3 and UHF-CCSD(T) methods, respectively. INT1 lies a few kcal mol^{-1} lower than TS-2. There are two possible pathways starting at INT1: it either dissociates via TS-2 back to the initial reactants, $NO_3 + N_2O$, or decomposes further via TS-3 to give products, $NO_2 + 2NO$. Given that the redissociation step faces a much lower barrier, it is expected to be dominant. As a result, the rate-determining step in this scenario is to surmount TS-3.

Statistical Rate Coefficient Calculations

Pathway 1: $NO_3 + N_2O \rightarrow$ TS-1 $\rightarrow NO_2 + N_2 + O_2$

As seen in Figure 1, when formed from the association of NO_3 with N_2O, Pre-1 rapidly re-dissociates back to reactants because the subsequent O-abstraction step must overcome a very high barrier. As a result, the canonical equilibrium, $NO_3 + N_2O \rightleftharpoons$ Pre-1, is quickly established before the following O-abstraction can occur. In addition, Post-1 – as produced by passing over TS-1 – has substantial internal energy, and thus rapidly decomposes to products, $NO_2 + N_2 + O_2$. Because of this, the influences of Pre-1 and Post-1 on chemical kinetics are negligible. Consequently, a kinetics scheme in this scenario can be simplified to: $NO_3 + N_2O \rightarrow$ TS-1 $\rightarrow NO_2 + N_2 + O_2$, which does not go through a long-lived intermediate, and therefore is expected to be pressure-independent. Thermal rate constants can be calculated using transition state theory (TST) [21, 22] at the high-pressure limit:

$$k_{TST}(T) = \frac{\sigma}{h} \times \frac{Q_{tr}^{\neq} Q_{e}^{\neq}}{Q_{NO_3}^{re} \cdot Q_{N_2O}^{re}} \times \sum_{J=0}^{\infty} (2J+1) \int_{0}^{\infty} G_{rv}^{\neq}(E,J) \exp(-E/k_B T)\, dE \qquad (1)$$

Where h is Planck's constant, k_B is Boltzmann's constant, and $\sigma = 12$ is the reaction path degeneracy. For the latter, note that rotational symmetry numbers are 6,1, and 1, respectively, for NO_3, N_2O, and TS-1. In addition, TS-1 is chiral and therefore has a mirror image. $Q_{NO_3}^{re}$ and $Q_{N_2O}^{re}$ are the complete partition functions for NO_3 and N_2O, respectively. Q_{tr} is the translational partition function and Q_e is the electronic partition function (the superscripts "re" and "≠" designate reactants and transition state, respectively). J is the

total angular momentum quantum number. $G_{rv}^{\neq}$ is the sum of rovibrational states for TS-1 obtained by convoluting vibrational and rotational quantum states [23]:

$$G_{rv}^{\neq}(E,J) = \int_0^E G_v^{\neq}(E - E_r)\rho_r^{\neq}(E_r)dE_r \quad (2)$$

Where $\rho_r^{\neq}(E_r)$ is the density of states at energy E_r. It is assumed that all stationary points on the potential energy surface are approximated by a rigid-rotor symmetric top [23], for which rotational energy levels are given by Eq. 3:

$$E_r(J,K) = J(J+1)\overline{B} + (A - \overline{B})K^2, \text{ with } \overline{B} = \sqrt{B \cdot C} \text{ and } -J \leq K \leq +J \quad (3)$$

With A, B, and C as the rotational constants. It should be mentioned that tunneling effects with an asymmetric Eckart model [24] are included in computing $G_v^{\neq}$ in Eq. 2 through Eq. 4[25]:

$$G_v^{\neq}(E) = \int_0^E P(x)_{Eckart} \times \rho_v^{\neq}(E - x)dx \quad (4)$$

Here P(x) is the asymmetric Eckart tunneling probability.

The rate constants calculated as a function of temperature are shown in Table 2. Inspection of Table 2 shows that k(T) increases sharply by about *sixty-three orders of magnitude* when temperature rises from 100 to 400 K, as expected for a reaction having a high reaction barrier. Because of the motion of the heavy oxygen atom, the tunneling

correction also increases significantly with decreasing temperature: it is a factor of ca. 4 at 300 K and becomes about 2×10^{19} at 100 K; but, even such a large tunneling enhancement is insufficient to overcome the very small rate constant caused by the high barrier. At room temperature, the calculated rate constant is 10^{-47} cm^3 $molecule^{-1}$ s^{-1}, which corresponds to a N_2O lifetime of 2×10^{38} seconds (about 10^{31} years), assuming an atmospheric $[NO_3] \approx 5\times10^8$ molecules/cm^3 [26]. Even if this rate coefficient were ten orders of magnitude larger, it would not make any contribution to the atmospheric removal of N_2O. At the lower temperatures, the rate coefficient will be even smaller. Therefore (even allowing for considerable uncertainty in our calculations), it can be safely concluded that reaction pathway 1 has absolutely no relevance in the atmosphere; it is most certainly not a potential sink for N_2O.

Pathway 2: $NO_3 + N_2O \rightarrow$ TS-2 $\rightarrow$ INT1 $\rightarrow$ TS-3 $\rightarrow NO_2 + 2NO$

As shown in Figure 1, the endothermic reaction pathway 2 to form $NO_2 + 2NO$ from $NO_3 + N_2O$ passes through an intermediate INT1, which does not have a long lifetime. Therefore, this pathway may (or may not) depend on pressure. If it does, a master equation analysis is required to compute rate constants as functions of both temperature and pressure. To check this idea, we have computed thermal rate constants at two extreme conditions: the low- and high-pressure limits where analytical solutions can be obtained through Eq. 5 and Eq. 6, respectively.

At the low-P limit [27, 28]:

$$k(T)_{P=0} = \frac{\sigma}{h} \times \frac{Q_{tr}^{\neq} Q_{e}^{\neq}}{Q_{NO_3}^{re} \cdot Q_{N_2O}^{re}} \times \sum_{J=0}^{\infty} (2J+1) \int_{0}^{\infty} G_{eff}^{\neq}(E,J) \exp(-E/k_B T)\, dE$$

(5a)

Here $G_{eff}^{\neq}$ is the effective sum of rovibrational quantum states, which is given by Eq. (5b):

$$G_{eff}^{\neq} = \frac{G_{TS2}^{\neq}(E,J) \times G_{TS3}^{\neq}(E,J)}{G_{TS2}^{\neq}(E,J) + G_{TS3}^{\neq}(E,J)} \quad (5b)$$

At the high-P limit [28]:

$$k(T)_{P=\infty} = \frac{k_2(T) \times k_3(T)}{k_{-2}(T) + k_3(T)} \quad (6)$$

Where $k_2(T)$ is the thermal rate constant for the forward step: $NO_3 + N_2O \rightarrow$ TS-2 $\rightarrow$ INT1, $k_{-2}(T)$ is the thermal rate constant for the reverse process: INT1 $\rightarrow$ TS-2 $\rightarrow NO_3 + N_2O$, and $k_3(T)$ is the thermal rate constant for the formation of the products: INT1 $\rightarrow$ TS-3 $\rightarrow NO_2 + 2NO$.

These three rate constants are computed using TST and presented in Table 3. Inspection of Table 3 shows that the loss of INT1 through TS-2 is many orders of magnitude faster than via TS-3, so that INT1 rapidly re-dissociates back to the initial reactants once it is produced. Consequently, INT1 has a very short lifetime that is not compatible with thermalization via collisions with a third body such as N_2 (and/or O_2) under atmospheric conditions. In other words, this reaction pathway is pressure-independent (also supported by the numbers in Table 4 where the difference between the low- and high-pressure rate constants is much smaller than 1%).

Comparison of the rate coefficient calculated at 298 K with the only reported value is useful. Cantrell et al. [2] measured the rate coefficient at P=1 atm in air. Their reported upper limit is consistent with our calculations, but it is to be noted that our value is many orders of magnitude smaller than their constraining limit.

Inspection of Table 4 shows that the calculated rate constants increase with temperature, as expected for a reaction having a high barrier. At room temperature, we obtain a rate constant of *ca.* 6×10^{-43} cm^3 $molecule^{-1}$ s^{-1} which, although five orders of magnitude faster than pathway 1, still leads to a calculated atmospheric lifetime of N_2O of *ca.* $\sim3\times10^{33}$ seconds (> 10^{26} years). Thus, taken together with our results for Reaction 1, the contribution of NO_3 reacting with N_2O to the lifetime of N_2O in the atmosphere is completely negligible. Even local influences of NO_3 on N_2O, and vice-versa, would be negligible. At lower atmospheric temperatures, the loss rate would be even smaller.

It is worth noting that our calculated thermal rate constants may be in error by a few orders of magnitudes due to numerous possible errors in our kinetics calculations that involve barrier heights, RRHO model, tunneling corrections, and so on. Yet, the main conclusion obtained from this study is that the loss of N_2O through either pathway 1 or pathway 2 is utterly negligible in Earth's atmosphere or even on a geological timescale.

DISCUSSION

As stated in the introduction, N_2O is one of the most important greenhouse gases, trailing only CO_2, CH_4 and water vapor in importance, and is believed to be the most important ozone-depleting substance of the 21st Century [1]. Its concentration in the atmosphere

has risen steadily in modern times (a roughly linear rise of ca. 0.8 ppb yr^{-1} [since 1980 [29]), which has been attributed at least in part to an increase in fertilized land use. If steps are not made to mitigate its anthropogenic sources (it also has natural sources), its importance as an atmospheric constituent will continue to increase. While it is known that N_2O can be destroyed by photolysis and via reaction with $O(^1D)$ atoms in the upper atmosphere – the modeling of which leads to its estimated atmospheric lifetime of 114 years [30] – other chemical sinks for the molecule are unknown. Accordingly, this is the second in a series of studies that investigate "slow" reactions of N_2O, done with an eye towards discovering potential chemical sinks that are relevant on a time scale of centuries to perhaps millenia. And this is also the second study to investigate a plausible reaction (the first being reaction of N_2O with the hydroxyl radical, OH [18]) to find that N_2O is exquisitely unreactive; lifetimes found so far are so long that they are several orders of magnitude greater than that of the universe itself.

It seems likely that N_2O is resistant to all potential chemical loss mechanisms in the atmosphere (apart from reaction with $O(^1D)$ in the stratosphere), and that it is simply a highly unreactive atmospheric molecule like CO_2. One could rationalize this by recognizing that it is isoelectronic with CO_2; decomposition reactions of the latter will lead to the *most stable* diatomic molecule (CO) while those of nitrous oxide lead to the *second most stable* diatomic molecule (N_2). Hence, the fact that both molecules lack chemical sinks in the troposphere is not particularly surprising; the consequence of such a situation is that N_2O will continue to grow in importance as a greenhouse gas, and is a molecule that is "here to stay".

CONCLUSIONS

Since it is very difficult to measure very slow free radical reactions, in this work we have estimated the rate coefficient for the potential reaction of NO_3 with N_2O using high-level quantum chemical and statistical chemical kinetics calculations. We find that there are potentially two reaction pathways, both of which have substantial barriers. The following kinetics analysis shows that these reactions are extremely slow and negligible in Earth's atmosphere. It should be noted that uncertainties of even 5 kcal mol^{-1} do not alter the conclusions regarding the loss of N_2O from the troposphere since the upper limits for the rate coeffients are so small.

Supplementary Material

Theoretical methods, optimized geometries, and rovibrational parameters for various stationary points are provided.

Acknowledgements

The work at University of Florida was supported by the U.S. National Science Foundation (Grant CHE-1664325) and Department of Energy, Office of Science, Office of Basic Energy Sciences under Award DE-FG02-07ER15884. Work of ARR was supported by Colorado State University and Le Studium Advanced Institute for Research, Loire Valley, Orleans, France.

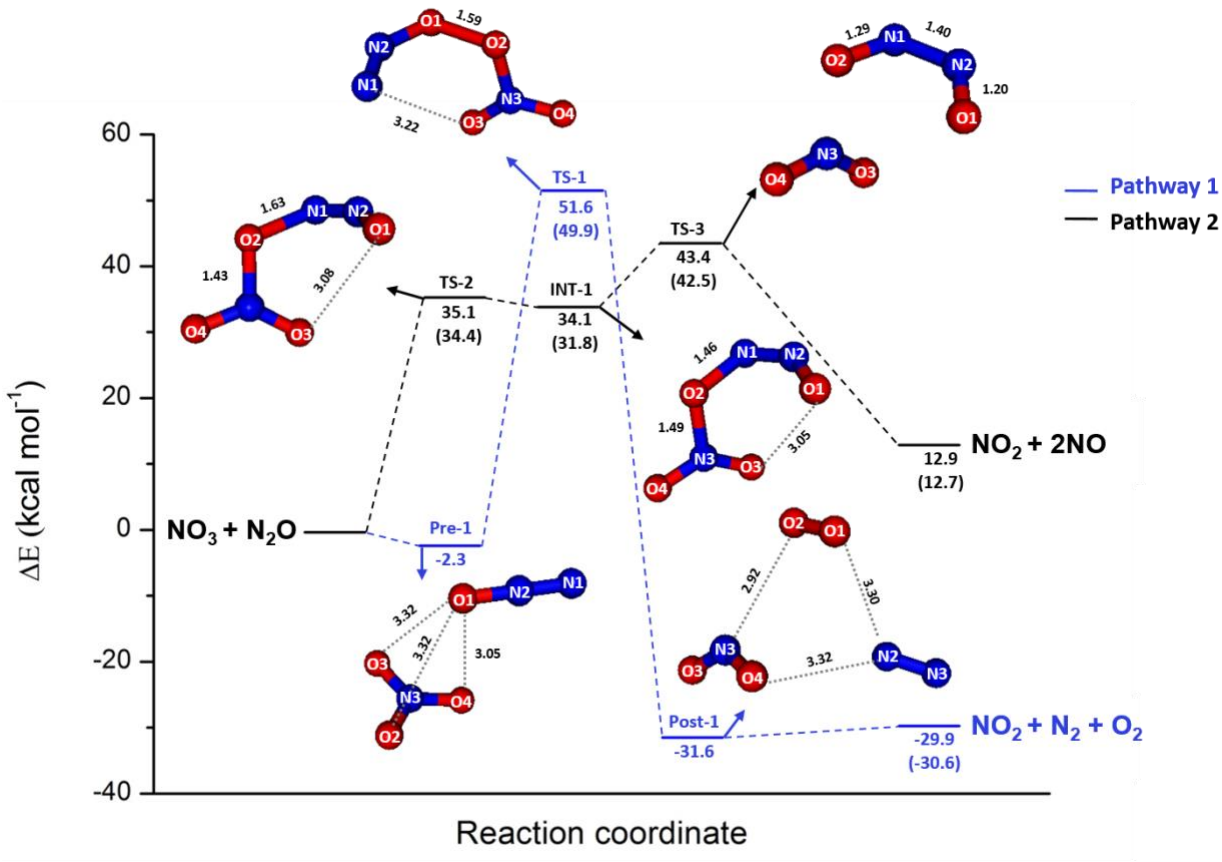

Figure 1: The potential energy surface for the reaction of NO_3 radical with N_2O calculated using the G3B3 method. The energy values given in parenthesis are obtained at the CCSD(T)/cc-pVQZ level of theory. The black and blue lines correspond to the endothermic and exothermic pathways respectively. The bond lengths are given in Å.

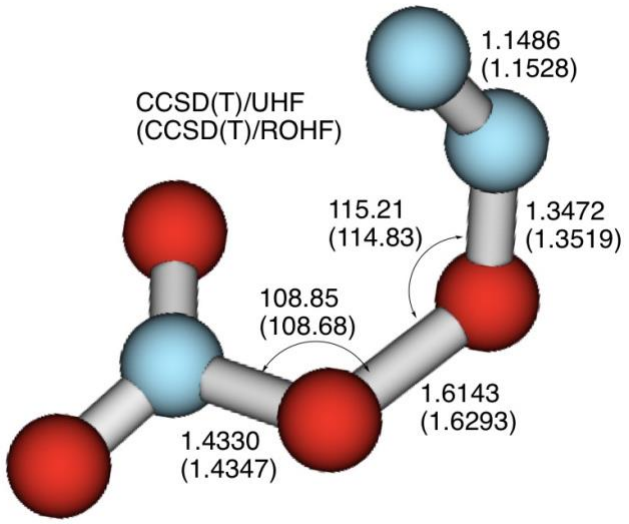

Figure 2: Geometrical parameters of TS-1 are optimized using UHF-CCSD(T)/ANO1 and ROHF-CCSD(T)/ANO1 (parenthesis) levels of theory. The energy at the ROHF-CCSD(T)/ANO1 level of theory is 2 kcal mol^{-1} lower than that of the other.

Table 1: Calculated relative energies (kcal mol^{-1}) of various species involved in the reaction of NO_3 with N_2O for the exothermic and endothermic channels.

$NO_3 + N_2O \rightarrow NO_2 + N_2 + O_2$			$NO_3 + N_2O \rightarrow NO_2 + 2NO$		
Species	G3B3	CCSD(T)/cc-pVQZ	Species	G3B3	CCSD(T)/cc-pVQZ
Pre-1	−2.3	-n/a-	TS-2	35.1	34.4
TS-1	51.6	49.9	INT1	34.1	31.8
Post-1	−31.6	-n/a-	TS-3	43.4	42.5
$NO_2 + N_2 + O_2$	−29.9 (−30.72 ± 0.1) [a]	−30.6 (−30.72 ± 0.1) [a]	$NO_2 + 2NO$	12.9 (12.60 ± 0.1) [a]	12.7 (12.60 ± 0.1) [a]

a) Taken from ATcT, version 1.122d, 2019 [31].

Table 2: Calculated thermal rate constants (cm^3 $molecule^{-1}$ s^{-1}) and tunneling corrections for the direct O-abstraction pathway 1: $NO_3 + N_2O \rightarrow N_2 + NO_2 + O_2$.

T (K)	CTST	CTST/Eckart	Tunneling correction
100	2.82×10^{-121}	6.04×10^{-102}	2.15×10^{19}
125	1.81×10^{-99}	4.94×10^{-87}	2.73×10^{12}
150	6.54×10^{-93}	5.38×10^{-85}	8.23×10^{7}
175	1.70×10^{-74}	1.10×10^{-69}	6.48×10^{4}
200	1.14×10^{-66}	6.14×10^{-64}	538
225	1.44×10^{-60}	5.16×10^{-59}	35.9
250	1.12×10^{-55}	1.14×10^{-54}	10.2
275	1.15×10^{-51}	6.20×10^{-51}	5.41
300	2.58×10^{-48}	9.56×10^{-48}	3.72
325	1.79×10^{-45}	5.18×10^{-45}	2.89
350	4.96×10^{-43}	1.20×10^{-42}	2.42
375	6.56×10^{-41}	1.39×10^{-40}	2.12
400	4.78×10^{-39}	9.10×10^{-39}	1.91

Table 3: Calculated individual thermal rate constants (in the reaction pathway 2) at the high-pressure limit.

T (K)	$k_2(T)$ in cm^3 $molecule^{-1}$ s^{-1}	$k_{-2}(T)$ in s^{-1}	$k_3(T)$ in s^{-1}
100	3.38×10^{-86}	4.89×10^{6}	3.84×10^{-7}
125	1.09×10^{-71}	2.07×10^{7}	1.60×10^{-5}
150	6.32×10^{-62}	6.44×10^{7}	8.56×10^{-4}
175	6.62×10^{-55}	1.56×10^{8}	3.59×10^{-2}
200	1.30×10^{-49}	3.14×10^{8}	8.45×10^{-1}
225	1.77×10^{-45}	5.51×10^{8}	1.13×10^{1}
250	3.70×10^{-42}	8.70×10^{8}	9.63×10^{1}
275	1.97×10^{-39}	1.27×10^{9}	5.74×10^{2}
300	3.76×10^{-37}	1.75×10^{9}	2.59×10^{3}

325	3.24×10^{-35}	2.29×10^{9}	9.38×10^{3}
350	1.50×10^{-33}	2.89×10^{9}	2.85×10^{4}
375	4.20×10^{-32}	3.52×10^{9}	7.49×10^{4}
400	7.86×10^{-31}	4.20×10^{9}	1.75×10^{5}

Table 4: Calculated rate constants (cm^3 $molecule^{-1}$ s^{-1}) at the low- and high-pressure limits for the addition/elimination reaction pathway 2: $NO_3 + N_2O \rightarrow O_2NONNO \rightarrow NO_2 + 2NO$

T (K)	Low-P limit [a]	High-P limit [b]	diff. (%) [c]
100	2.6460×10^{-99}	2.6460×10^{-99}	0
125	8.4208×10^{-84}	8.4208×10^{-84}	0
150	8.4022×10^{-73}	8.4022×10^{-73}	0
175	1.5226×10^{-64}	1.5226×10^{-64}	0
200	3.4888×10^{-58}	3.4894×10^{-58}	1.33×10^{-2}
225	3.6344×10^{-53}	3.6354×10^{-53}	2.48×10^{-2}
250	4.0874×10^{-49}	4.0890×10^{-49}	4.09×10^{-2}
275	8.8806×10^{-46}	8.8862×10^{-46}	6.23×10^{-2}
300	5.5558×10^{-43}	5.5616×10^{-43}	8.99×10^{-2}
325	1.3233×10^{-40}	1.3269×10^{-40}	1.25×10^{-1}
350	1.4762×10^{-38}	1.4787×10^{-38}	1.67×10^{-1}
375	8.9186×10^{-37}	8.9380×10^{-37}	2.18×10^{-1}
400	3.2716×10^{-35}	3.2808×10^{-35}	2.78×10^{-1}

a) Eq. 5 in the main text.
b) Eq. 6 in the main text.
c) Difference (%) = $[k(T,P=\infty) - k(T,P=0)] \times 100\% / k(T,P=\infty)$

References

[1] A.R. Ravishankara, J.S. Daniel, R.W. Portmann, Nitrous Oxide (N2O): The Dominant Ozone-Depleting Substance Emitted in the 21st Century, Science 326 (2009) 123-125.

[2] C.A. Cantrell, J.A. Davidson, R.E. Shetter, B.A. Anderson, J.G. Calvert, Reactions of nitrate radical and nitrogen oxide (N2O5) with molecular species of possible atmospheric interest, The Journal of Physical Chemistry 91 (1987) 6017-6021.

[3] A. Tajti, P.G. Szalay, A.G. Csaszar, M. Kallay, J. Gauss, E.F. Valeev, B.A. Flowers, J. Vazquez, J.F. Stanton, HEAT: High accuracy extrapolated ab initio thermochemistry, J Chem Phys 121 (2004) 11599-11613.

[4] Y.J. Bomble, J. Vazquez, M. Kallay, C. Michauk, P.G. Szalay, A.G. Csaszar, J. Gauss, J.F. Stanton, High-accuracy extrapolated ab initio thermochemistry. II. Minor improvements to the protocol and a vital simplification, J Chem Phys 125 (2006).

[5] M.E. Harding, J. Vazquez, B. Ruscic, A.K. Wilson, J. Gauss, J.F. Stanton, High-accuracy extrapolated ab initio thermochemistry. III. Additional improvements and overview, J Chem Phys 128 (2008).

[6] A.G. Baboul, L.A. Curtiss, P.C. Redfern, K. Raghavachari, Gaussian-3 theory using density functional geometries and zero-point energies, J Chem Phys 110 (1999) 7650-7657.

[7] L.A. Curtiss, K. Raghavachari, P.C. Redfern, A.G. Baboul, J.A. Pople, Gaussian-3 theory using coupled cluster energies, Chem Phys Lett 314 (1999) 101-107.

[8] K. Fukui, The Path of Chemical-Reactions - the Irc Approach, Accounts Chem Res 14 (1981) 363-368.

[9] H.P. Hratchian, H.B. Schlegel, Accurate reaction paths using a Hessian based predictor-corrector integrator, J Chem Phys 120 (2004) 9918-9924.

[10] H.P. Hratchian, H.B. Schlegel, Using Hessian updating to increase the efficiency of a Hessian based predictor-corrector reaction path following method, Journal of Chemical Theory and Computation 1 (2005) 61-69.

[11] M.J. Frish, G.W. Trucks, H.B. Schlegel, G.E. Scuseria, M.A. Robb, e. al., Gaussian 09, Revision D.01, In Wallingford CT, 2009.

[12] J.F. Stanton, Why CCSD(T) works: a different perspective, Chem Phys Lett 281 (1997) 130-134.

[13] K. Raghavachari, G.W. Trucks, J.A. Pople, M. Headgordon, A 5th-Order Perturbation Comparison of Electron Correlation Theories, Chem Phys Lett 157 (1989) 479-483.

[14] R.J. Bartlett, J.D. Watts, S.A. Kucharski, J. Noga, Noniterative 5th-Order Triple and Quadruple Excitation-Energy Corrections in Correlated Methods, Chem Phys Lett 165 (1990) 513-522.

[15] J. Almlof, P.R. Taylor, General Contraction of Gaussian-Basis Sets .1. Atomic Natural Orbitals for 1st-Row and 2nd-Row Atoms, J Chem Phys 86 (1987) 4070-4077.

[16] J. Almlof, P.R. Taylor, General Contraction of Gaussian-Basis Sets .2. Atomic Natural Orbitals and the Calculation of Atomic and Molecular-Properties, J Chem Phys 92 (1990) 551-560.

[17] T.H. Dunning, Gaussian-Basis Sets for Use in Correlated Molecular Calculations .1. The Atoms Boron through Neon and Hydrogen, J Chem Phys 90 (1989) 1007-1023.

[18] T.L. Nguyen, A.R. Ravishankara, J.F. Stanton, Analysis of the potential atmospheric impact of the reaction of N2O with OH, Chem Phys Lett 708 (2018) 100-105.

[19] J.F. Stanton, e. al., CFOUR, a quantum chemical program package, For the current version, see http://www.cfour.de.
[20] S.P. Sander, R.R. Friedl, J.R. Barker, D.M. Golden, M.J. Kurylo, P.H. Wine, J.P.D. Abbatt, J.B. Burkholder, C.E. Kolb, G.K. Moorgat, R.E. Huie, V.L. Orkin, JPL Evaluation number 17: Chemical Kinetics and Photochemical Data for Use in Atmospheric Studies, (2011).
[21] H. Eyring, The activated complex in chemical reactions, J Chem Phys 3 (1935) 107-115.
[22] M.G. Evans, M. Polanyi, Some applications of the transition state method to the calculation of reaction velocities, especially in solution., T Faraday Soc 31 (1935) 0875-0893.
[23] T. Baer, W.L. Hase, Unimolecular reaction dynamics : theory and experiments, Oxford University Press, New York, 1996.
[24] W.H. Miller, Tunneling Corrections to Unimolecular Rate Constants, with Application to Formaldehyde, J Am Chem Soc 101 (1979) 6810-6814.
[25] W. Forst, Unimolecular reactions : a concise introduction, Cambridge University Press, Cambridge, U.K. ; New York, 2003.
[26] R. Atkinson, Gas-Phase Tropospheric Chemistry of Volatile Organic Compounds: 1. Alkanes and Alkenes, J. Phys. Chem. Ref. Data 26 (1997) 215-290.
[27] W.H. Miller, Unified Statistical-Model for Complex and Direct Reaction-Mechanisms, J Chem Phys 65 (1976) 2216-2223.
[28] T.L. Nguyen, B.C. Xue, R.E. Weston, J.R. Barker, J.F. Stanton, Reaction of HO with CO: Tunneling Is Indeed Important, J Phys Chem Lett 3 (2012) 1549-1553.
[29] T.M. Thompson, Halocarbons and other atmospheric trace
species. In: Climate Monitoring and Diagnostics Laboratory, Summary
Report No. 27 [Schnell, R.C., A.-M. Buggle, and R.M. Rosson (eds.)].
NOAA CMDL, Boulder, CO, pp. 115–135., (2004).
[30] S.A. Montzka, Controlled substances and other source gases. In: Scientifi c Assessment of Ozone Depletion: 2002. World Meteorological Organization, Geneva, pp. 1.1–1.83, (2003).
[31] B. Ruscic, D.H. Bross, Active Thermochemical Tables (ATcT) values based on ver. 1.122d of the Thermochemical Network (2018), available at ATcT.anl.gov, 2018.